Master of Science Thesis

Geometric Control of a Quadrotor with a Suspended Load

N.N. Vo

June 26, 2017

Delft Center for Systems and Control

Delft University of Technology

Geometric Control of a Quadrotor with a Suspended Load

Master of Science Thesis

For obtaining the degree of Master of Science in Mechanical Engineering at Delft University of Technology

N.N. Vo

June 26, 2017

Faculty of Mechanical, Maritime and Materials Engineering · Delft University of Technology

The work in Master of Science Thesis was supported by Alten. Their cooperation is hereby gratefully acknowledged.

Delft University of Technology

Delft University Of Technology
Delft Center for Systems and Control

The undersigned hereby certify that they have read and recommend to the Faculty of Mechanical, Maritime and Materials Engineering for acceptance a thesis entitled **"Geometric Control of a Quadrotor with a Suspended Load"** by **N.N. Vo** in partial fulfillment of the requirements for the degree of **Master of Science**.

Dated: June 26, 2017

Supervisor: _____
dr.ir. T. Keviczky

Readers: _____
ir. B. van Vliet

Abstract

A Quadrotor is a type of Unmanned Aerial Vehicle that has received an increasing amount of attention recently with many applications including search and rescue, surveillance, supply of food and medicines as disaster relief and object manipulation in construction and transportation. An interesting subproblem of transportation, is the control of the position of a cable suspended load. The challenge is in the fact that the Quadrotor-Load system is highly nonlinear and under-actuated. The load cannot be controlled directly and has a natural swing at the end of each Quadrotor movement.

This thesis presents a Nonlinear Geometric Control approach for the position tracking of a cable suspended load. In this work the dynamical model of the Quadrotor-Load system is limited to the subsystem where the cable tension is non-zero, which is analogous to modeling a rigid link between the Quadrotor and Load. Based on the geometric properties of the system, Geometric Mechanics apply differential geometric techniques to systems modeling and control. The Quadrotor-Load system dynamics are modeled on so called manifolds, smooth nonlinear geometric configuration spaces. Analyzing these geometric structures with the principles of differential geometry allows modeling in an unambiguous coordinate-free dynamic fashion, while avoiding the problem of singularities that would occur on local charts. Tracking error functions are defined on these same spaces, making it possible to design almost globally defined controllers.

The main goal of this thesis is to investigate the possibilities and limitations of Nonlinear Geometric Control by evaluating the performance of tracking different load trajectories. A backstepping approach is applied to generate a cascaded structure with multiple nonlinear Geometric controllers, allowing control of several flight modes that are responsible for the control of 1) Quadrotor attitude, 2) Load attitude and 3) Load position. A Linear Quadratic Regulator is derived to compare control performance. Simulations are presented and the results of both the linear and nonlinear controller are discussed.

Acknowledgements

I would like to thank my supervisors dr.ir. T. Keviczky from Delft Center of Systems and Control, and ir. B. van Vliet from Alten Nederland B.V. for their assistance during my research and the writing of this thesis. I would also like to thank all colleagues from Alten and TU Delft for their time and advice.

Delft, University of Technology N.N. Vo
June 26, 2017

Table of Contents

List of Figures

List of Tables

Chapter 1

Introduction

A Quadrotor (QR) is a type of Unmanned Aerial Vehicle (UAV) that has received an increasing amount of attention recently with many applications being actively investigated. Possible applications include search and rescue, surveillance, reliable supply of food and medicines as disaster relief and object manipulation in construction and transportation. It has already proven itself useful for many tasks like multi-agent missions, mapping, explorations, transportation and entertainment such as acrobatic performances.

The inspiration for this research is build upon the idea of creating a system of multiple autonomous QRs for a cooperative towing task. The advantage of such a system for object manipulation is the possibility to reduce complexity of the individual robot, decrease cost over traditional robotic systems and high reliability. One can think of examples in nature, where individuals coordinate, cooperate and collaborate to perform tasks that they individually can not accomplish. Redundancy makes development of fail safe control methods possible and can extend the capabilities of a single robot.

Considering a multi-agent task, one can think of multiple QRs assisting in the transportation of a common load. This cooperation can be executed in many ways, but this research focuses on QRs with a cable-suspended load in motion. The suspended object naturally continues to swing at the end of every movement. In case a residual motion can result in damage or in order to avoid obstacles and path following, an accurate positioning is required. Reducing the oscillation, or controlling the position of the suspended load might be necessary, but is challenging in the fact that this cable-suspended system is under-actuated. Possible objectives are minimizing the oscillations of the load during or after motion, minimizing the time to position the load, trajectory tracking, trajectory generation and obstacle avoidance.

1-1 Aim and Motivation

The aim is to control the position of a suspended load using a QR. Before considering multiple QRs, it is important to investigate the possibilities of a single QR with load system. Hence, in this research a single QR is considered for the transportation of a cable suspended load, which will exert additional forces and torques on the QR. This is a challenging control problem in the fact that the QR system is under-actuated. Adding a suspended load will add extra DOFs and oscillations of the load occur at the end of every movement.

The system can be divided into two subsystems. The first subsystem is where the cable tension is non-zero and the distance between the QR and the load is defined by the cable length. Both QR and load are coupled as one system. The second subsystem is where the cable tension is zero, such that the QR and load in free fall are two separate decoupled systems. This research focuses on the first subsystem, such that the cable tension is non-zero. In order to control both subsystems, hybrid control must be applied, which is considered out of the scope of this research.

Former work on attitude control of QR and/or load often relies on linear control methods such as PID, MPC and LQR control. The dynamics are linearized around an equilibrium point, describing the system dynamics by a set of linear differential equations. The control of a QR-Load system is a very specific case and scarcely investigated. Former work includes MPC [1] and LQR control approaches, where an optimal control strategy is used to minimize the swing of the load.

The reason that linear control near an equilibrium state is commonly applied, is partly to avoid difficulties that come with modeling and controlling the non-linearities of the system. However, linear control limits the system to small angle movements, as the optimization will not allow large angles that deviate to far from the linearized point. For applications that require fast aggressive maneuvers, this type of modeling and control will not be sufficient. Nonlinear control systems are often governed by nonlinear differential equations and are able to represent the dynamics in a more realistic manner. Nonlinear control approaches to minimize the load swing includes a Model Based Algorithm controller applied by [2].

Nonlinear Geometric Control is a nonlinear model based control technique based on a modeling approach involving the concepts of differential geometry. This results in a globally defined coordinate-free dynamical model, while preventing issues regarding singularities, and enabling the design of controllers that offer almost-global convergence properties.

Former work includes a nonlinear geometric control of a QR [3, 4] and nonlinear geometric control of the load position, load attitude and QR attitude of a QR-Load system [5, 6, 7]. Nonlinear Geometric Control for QR systems is rarely found in literature, despite the advantageous properties of differential geometry.

This motivates to investigate the possibilities and limitations of a rarely used nonlinear Geometric Control approach, and to investigate the performance of a load transportation maneuver, when compared to a commonly used linear control strategy.

Different aspects involving the modeling and control for the QR-Load system must be investigated, for it can be expected that the non-linearity will have a great influence in the representation of the dynamics and the stability, accuracy and type of the control design.

It is possible to investigate which advantages or disadvantages this nonlinear approach has compared to a linear approach, in terms of stability and performance.

System consists of two sub-systems Limited to subsystem where the tension of the cable is non-zero.

1-2 Organization of the Report

In this first chapter, a brief introduction of the subject is given and the problem is described. This is followed by discussing the aim, motivation and contributions of this thesis for this research. The organization of the report is as follows.

In Chapter 2 the dynamics of the QR-Load system is described by the laws of kinematics and the application of Newton's laws or Lagrangian mechanics. Geometric Mechanics is used to understand and derive the equations of motion of the system in order to allow analysis and controller design. The system configuration space is described on a differentiable manifold using the tools of Differential geometry, creating a compact, unambiguous and coordinate-free model. opposed to classical modeling techniques, where the system dynamics evolve in a three dimensional space using the tools of Euclidean geometry.

The system dynamics are represented on nonlinear manifolds and this allows nonlinear geometric controllers to be designed on these same manifolds. The control design is presented in Chapter 3. The controller has a cascaded structure, where the different control loops are accountable for different flight modes.

Different tracking objectives are defined in order to compare the performance between an LQR control design and a nonlinear Geometric Control design. Chapter 5 describes the experiments that are done to investigate the abilities and performance of a nonlinear Geometric Control design. The results and findings are presented and discussed.

In the final chapter a summary of the thesis is given, followed by the conclusions that were made based on the results of the experiments. Finally, recommendations are given which could serve as an starting point for future work.

Chapter 2

Dynamic Model

A mathematical model of the system needs to be derived in order to simulate and study the effects of nonlinear Geometric Control. In Section 2-1 an introduction is given about Geometric Mechanics. This is a modern description of the classical mechanics from the perspective of Differential Geometry, which is a discipline in mathematics that studies manifolds and their geometric properties, using the tools of calculus.

The assumptions that are applied to simplify the model are shortly discussed in Section 2-2. Next, in Section 2-3 a dynamical model of the QR-Load system is obtained with Geometric Mechanics, resulting in a compact, coordinate-free, unambiguous representation of the dynamics, described on nonlinear manifolds.

2-1 Geometric Mechanics

To derive the equations of motions, traditional modeling methods often parameterize the rotations in a local coordinate system. This can be done with Euler Angles, and despite this parametrization might result in singularities, this is a commonly used method to describe rotations. There are 24 possible sets of Euler angles and many different conventions are used, which introduces ambiguity. The definition of Euler angles is not unique and a sequence of rotations is not commutative. Therefore, Euler angles are never expressed in terms of the external frame, or in terms of the co-moving rotated body frame, but in a mixture.

Euler angles are kinematically singular since the transformation from their time rates of change to the angular velocity vector is not globally defined. Furthermore, when angular errors are large, the difference in Euler angles is no longer a good metric to define the orientation error. Hence, the error is rather written as the required rotation to get from the current to a desired orientation, which can be achieved by considering geometric properties of the system.

In Geometric Mechanics the configuration space of systems is a *group manifold* instead of a Euclidean space. The kinetic and potential energies are expressed in terms of this configuration space and their tangent spaces. It explores the geometric structure of a Lagrangian-

or Hamiltonian system through the concepts of vector calculus, linear algebra, differential geometry, and nonlinear control theory. Geometric mechanics provides fundamental insights into the nonlinear system mechanics and yields useful tools for dynamics and control theory.

To illustrate different configuration spaces, an example is given of a simple 2-link arm, see Figure 2-1a. The configuration is defined by the angles of rotation q_1 and q_2. Figure 2-1b represents the configuration space in a Cartesian coordinate system, where the markers represent identical configurations. This shows that this representation suffers from singularities where multiple points in one representation are being mapped onto a single point in another representation. Figure 2-1c represents the configuration space as a geometric shape called a *torus*, a smooth manifold where every configuration is mapped uniquely.

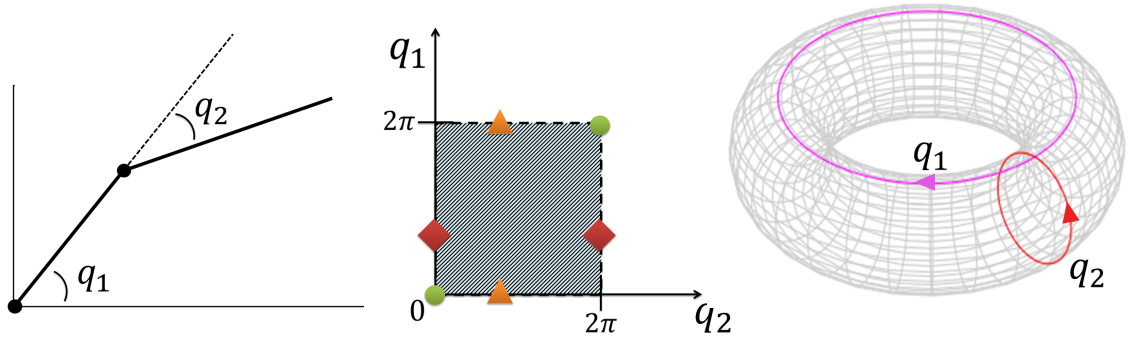

(a) (b) (c)

Figure 2-1: Configuration Space of a 2-link arm

Manifolds The fundamental object of differential geometry a manifold. A manifold is a mathematical space, a collection of points, that locally resembles Euclidean space near each point. Examples are a plane, a ball, a torus and a sphere. Manifolds are important objects in mathematics and physics because they allow more complicated structures to be expressed and understood in terms of the relatively well-understood properties of simpler spaces. In Figure 2-2 is illustrated that each point of an n-dimensional manifold has a neighborhood that is homeomorphic to the n-dimensional Euclidean space, meaning that there is a continuous function describing the relation between these spaces.

A differentiable manifold is a smooth and continuous manifold and is locally similar enough to a linear space to allow to do calculus. One can define directions, tangent spaces, and differentiable functions on such a manifold. Taking the derivative at a point on a manifold is equivalent to a tangent vector at that point. Meaning that derivatives are conceptually equivalent to an infinitesimally short tangent vector. Each point of an n-dimensional differentiable manifold has a tangent space, which is an n-dimensional Euclidean space consisting of all the tangent vectors of all curves that pass through that point.

In Figure 2-3a the manifold $\mathbb{S}^2$ is represented as a sphere, with a tangent space at point x, denoted by $T_x\mathbb{S}^2$. This illustrates the concept of the relation between v, the derivative of x in Cartesian space, and the tangent space in on the manifold.

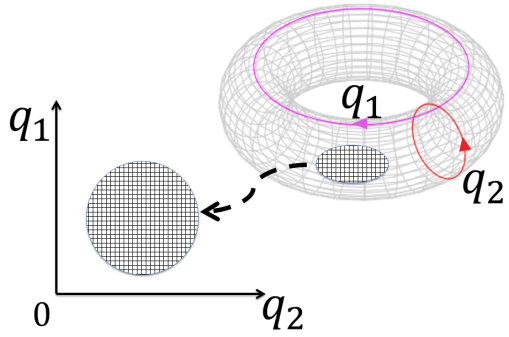

Figure 2-2: A manifold locally resembles a Euclidean space

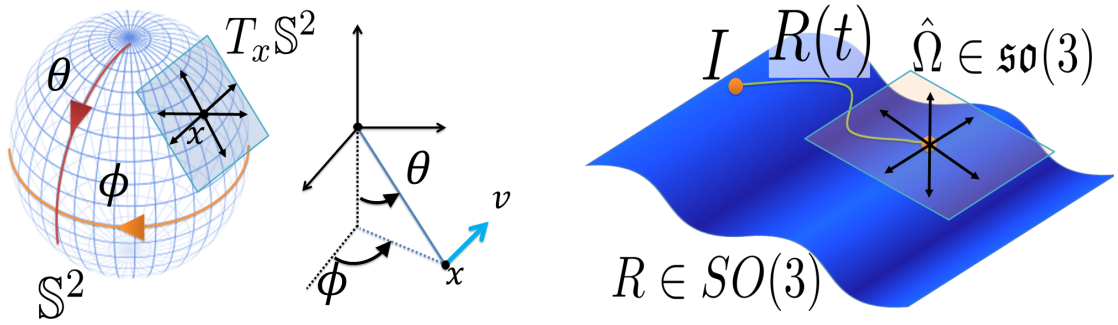

(a) Representation of a manifold with a tangent space

(b) Identity map of $SO(3)$ with Lie Algebra $\mathfrak{so}(3)$

Figure 2-3: Manifolds and Tangent Spaces

Configuration Spaces Rotation matrices are used to provide a global representation of the attitude of a rigid body, by mapping a representation of vectors expressed in $\{\mathcal{B}\}$ to a representation expressed in $\{\mathcal{I}\}$ [8, 9]. The configuration of the QR attitude is a rotation matrix R in the Special Orthogonal Group $SO(3)$ defined as

$$SO(3) \triangleq \left\{R \in \mathbb{R}^{3\times 3} | RR^T = I_{3\times 3}, det(R) = 1\right\} \tag{2-1}$$

$SO(3)$ is the group of all rotations about the origin of a 3-D Euclidean space, which preserves the origin, Euclidean distance and orientation. Several methods exist to describe rotations, such as *Euler Angles*, quaternions or rotation matrices. The main disadvantages of Euler angles are that some functions have singularities and they are a less accurate measure for the integration of incremental changes in attitude over time, compared to other methods. In Geometric Mechanics the rotations are expressed in rotation matrices to avoid these problems.

Every rotation has a unique inverse rotation and the identity map satisfies the definition of a rotation. The elements of *Lie Algebra* $\mathfrak{so}(3)$, a property associated with $SO(3)$, are the elements of the tangent space of $SO(3)$ at the identity element, see Figure 2-3b. These

elements define the relation between the rotation R and its derivative $\dot{R}$, such that

$$\dot{R} = R\hat{\Omega} \tag{2-2}$$

For $n \in \mathbb{N}$, $\mathfrak{so}(3)$ is is the vector space of skew-symmetric matrices in $\mathbb{R}^{n\times n}$ and defined as

$$\mathfrak{so}(n) \triangleq \left\{S \in \mathbb{R}^{n\times n} | S^T = -S\right\} \tag{2-3}$$

The linear map $\hat{\cdot} : \mathbb{R}^3 \to \mathfrak{so}(3)$ is an isomorphism between $\mathbb{R}^3$ and the set of 3×3 skew symmetric matrices. $\cdot^\vee : \mathfrak{so}(3) \to \mathbb{R}^3$ denotes the inverse isomorphism. The mapping between the body angular velocity vector $\Omega \in \mathbb{R}^3$ and $\hat{\Omega} \in \mathfrak{so}(3)$ can be written as

$$\hat{\Omega} = \begin{bmatrix} 0 & -\Omega_3 & \Omega_2 \\ \Omega_3 & 0 & -\Omega_1 \\ -\Omega_2 & \Omega_1 & 0 \end{bmatrix}, \quad \begin{bmatrix} 0 & -\Omega_3 & \Omega_2 \\ \Omega_3 & 0 & -\Omega_1 \\ -\Omega_2 & \Omega_1 & 0 \end{bmatrix}^\vee = \Omega \tag{2-4}$$

The configuration space of the load is represented on a 2-sphere, defined as

$$\mathbb{S}^2 \triangleq \left\{q \in \mathbb{R}^3 | q \cdot q = 1\right\} \tag{2-5}$$

$$\dot{q} = \omega \times q \tag{2-6}$$

where ω is the angular velocity of the suspended load.

2-2 Modeling Assumptions

The QR model representation is shown in Figure 2-4. Three Cartesian coordinate frames are defined:

- The body-fixed reference frame $\{\mathcal{B}\}$ (Body Frame)
  with unit vectors $\{\mathbf{b}_1, \mathbf{b}_2, \mathbf{b}_3\}$ along the axes
- The ground-fixed reference frame $\{\mathcal{I}\}$ (Inertial Frame)
  with unit vectors $\{\mathbf{e}_1, \mathbf{e}_2, \mathbf{e}_3\}$ along the axes
- The intermediary frame $\{\mathcal{C}\}$, ($\{\mathcal{I}\}$ rotated by the yaw angle ψ)
  with unit vectors $\{\mathbf{c}_1, \mathbf{c}_2, \mathbf{c}_3\}$ along the axes

The complex dynamics of the rotors and their interactions with drag and thrust forces are represented by a simplified model. The angular speed ω_i of rotor i, for $i = 1, \ldots, 4$, generates a force F_i parallel to the direction of the rotor axis of rotor i, given by

$$F_i = \left(\frac{K_v K_\tau \sqrt{2\rho A}}{K_t}\omega_i\right)^2 = b\omega_i^2 \tag{2-7}$$

where K_v, K_t are constants related to the motor properties, ρ is the density of the surrounding air, A is the area swept out by the rotor, K_τ is a constant determined by the blade configuration and parameters, and b is the thrust factor.
The torque around the axis of rotor i, for $i = 1, \ldots, 4$, generated due to drag is given by

$$M_i = \frac{1}{2}R\rho C_D A(\omega_i R)^2 = d\omega_i^2 \tag{2-8}$$

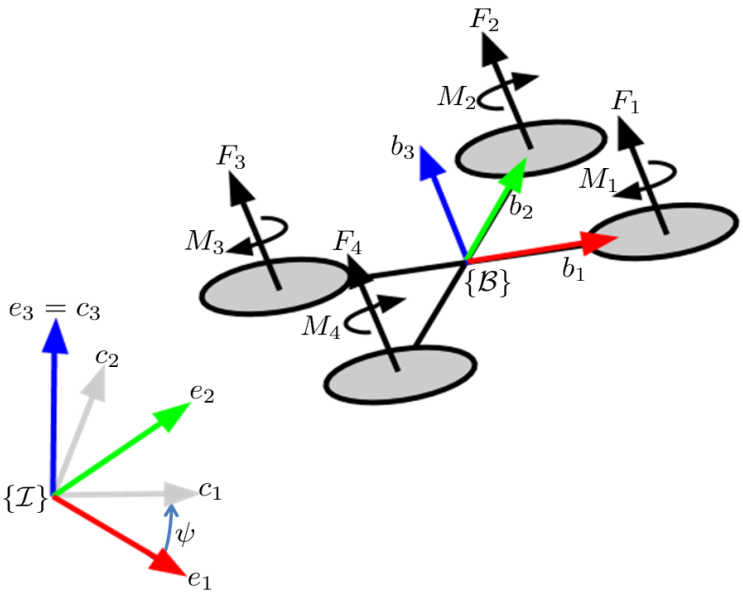

Figure 2-4: Quadrotor model representation

where R is the radius of the propeller, C_D is a dimensionless constant, and d is the drag constant.

For given desired total thrust f and total moment $M = \begin{bmatrix} M_\phi & M_\theta & M_\psi \end{bmatrix}^T$, the required rotor speeds can be calculated by solving the following equation

$$\begin{bmatrix} f \\ M_\phi \\ M_\theta \\ M_\psi \end{bmatrix} = \begin{bmatrix} b & b & b & b \\ 0 & -lb & 0 & lb \\ lb & 0 & -lb & 0 \\ -d & d & -d & d \end{bmatrix} \begin{bmatrix} \omega_1^2 \\ \omega_2^2 \\ \omega_3^2 \\ \omega_4^2 \end{bmatrix} \tag{2-9}$$

where l is the distance from the rotor to the QR's CoM and M_ϕ, M_θ, M_ψ denote the moments around the x, y, z-axis in $\{\mathcal{B}\}$, respectively.

Table 2-1 shows the most common assumptions that are used for modeling the QR, simplifying the complexity of the model.

2-3 Quadrotor-Load Model

The Quadrotor-Load model is shown in Figure 2-5, where the unit vector q gives the direction from the QR to the Load expressed in $\{\mathcal{B}\}$. The focus lies on the subsystem where the cable tension is considered to be non-zero. The position of the QR and Load are related by

$$x_Q = x_L - Lq \tag{2-10}$$

where x_Q is the position of the QR's CoM, x_L is the position of the load, and L is the length of the cable.

Considering the properties of the system, the QR is described as a rigid body with six degrees of freedom, driven by forces and moments. Dynamics and optimal control problems for rigid

Modeling assumptions Quadrotor model
• The structure of the QR is rigid and symmetric. Elastic deformations and shock (sudden accelerations) of the QR are ignored. • The mass distribution of the QR is symmetrical in the x-y plane. • The inertia matrix is time-invariant. • Aerodynamic effects acting on the QR are neglected. Blade flapping, Turbulence, Ground Effects. • The air density around the QR is constant. • The propellers are rigid ⇒ The thrust produced by rotor i is parallel to the axis of rotor i. • Drag factor d and thrust factor b are approximated by a constant. Thrust force F_i and moment M_i of each propeller is proportional to the square of the propeller speed.
Modeling assumptions Quadrotor-Load model
• The cable is modeled as a rigid and massless cable. • The cable is connected to a friction-less joint at the origin of the body-fixed. • The tension in the cable is considered to be non-zero. This implies that the QR-Load subsystem, consisting of a separate QR and Load in free fall, is disregarded. • Aerodynamic effects acting on the load are neglected. reference frame.

Table 2-1: Modeling assumptions

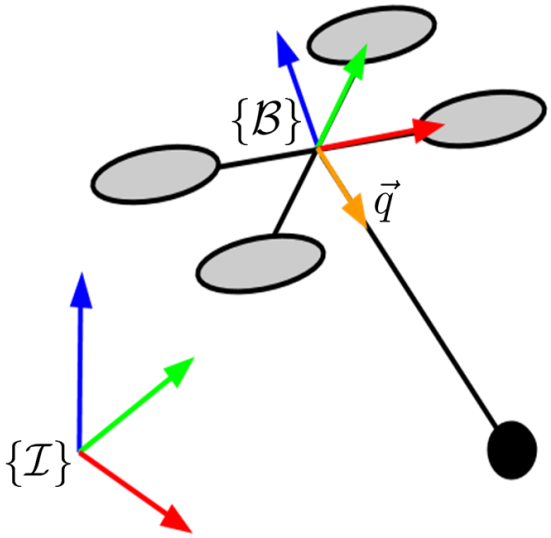

Figure 2-5: Quadrotor with Load model representation

bodies are studied in [10], incorporating their geometric features. The focus lies on obtaining geometric properties of the dynamics of rigid bodies, how their configuration can be described and how these geometric properties are utilized in control system analysis and design.

The configuration of the QR can be described by the location of the QRs CoM $x_Q \in \mathbb{R}^3$,

described in the Euclidean space in $\{\mathcal{I}\}$ and by the orientation of $\{\mathcal{B}\}$, also called attitude, with respect to $\{\mathcal{I}\}$ evolving on a nonlinear space $R \in SO(3)$.
The configuration of the load can be described by its location $x_L \in \mathbb{R}^3$, evolving in Euclidean space, and attitude $q \in \mathbb{S}^2$ evolving on a *two-sphere*.
This results that the dynamics of the QR-Load system can be globally expressed on the Special Orthogonal Group $SO(3)$, *two-sphere* $\mathbb{S}^2$ and Special Euclidean Group $SE(3)$. This leads to a compact notation of the equations of motion, making the large amount of trigonometric functions unnecessary, that Euler angles normally introduce.

To develop the Euler-Lagrange equations for mechanical systems that evolve on manifolds, an approach developed by [10, 11, 12, 13] is applied.

The basic idea is the variations of the curves that are e

This approach is based on Hamilton's principle, which states that the evolution of a physical system is a solution of the functional equation given by

$$\frac{\delta S}{\delta \mathbf{q}(t)} = 0 \tag{2-11}$$

where $\mathbf{q}$ defines the configuration space. S is the action integral, defined as

$$S = \int_{t_1}^{t_2} \mathcal{L} dt \tag{2-12}$$

where $\mathcal{L} = \mathcal{T} - \mathcal{U}$ is the Lagrangian of the system, and $\mathcal{T}$,$\mathcal{U}$ are the kinetic and potential energy, respectively.

Hamilton's principle of least action states that the path a conservative mechanical system takes between two configurations q_1 and q_2 at time t_1 and t_2, is the one for which Equation 2-12 is a stationary point, resulting in

$$\delta S = \int_{t_1}^{t_2} \delta \mathcal{L} dt = 0 \tag{2-13}$$

where $\delta\mathcal{L}$ is the variation of the Lagrangian. For systems with non-conservative forces and moments, Equation 2-13 is extended to

$$\delta S = \int_{t_1}^{t_2} (\delta W + \delta \mathcal{L}) dt = 0 \tag{2-14}$$

where δW is the virtual work. Equation 2-14 is applied to the QR-Load system, where the configuration manifold is $\mathbb{R}^3 \times \mathbb{S}^2 \times SO(3)$. With the following states

$$\mathbf{x} = \begin{bmatrix} x_L & \dot{x}_L & q & \omega & R & \Omega \end{bmatrix}^T \tag{2-15}$$

Euler-Lagrange Equation 2-13 can be satisfied if the following Euler-Lagrange equation holds

$$\frac{\delta \mathcal{L}}{\delta \mathbf{q}} - \frac{d}{dt} \frac{\delta \mathcal{L}}{\delta \dot{\mathbf{q}}} = 0 \tag{2-16}$$

where the Lagrangian $\mathcal{L} = \mathcal{T} - \mathcal{U}$. The kinetic energy for the system is denoted as

$$\mathcal{T} = \frac{1}{2} m_Q \dot{x}_Q \cdot \dot{x}_Q + \frac{1}{2} m_L \dot{x}_L \cdot \dot{x}_L + \frac{1}{2} \Omega \cdot J \cdot \Omega \tag{2-17}$$

and the potential energy is denoted as

$$\mathcal{U} = m_Q g x_Q \cdot e_3 + m_L g x_L \cdot e_3 \tag{2-18}$$

where g is the gravity constant. The energy can be rewritten in terms of q and x_L, by substituting Equation 2-10, giving

$$\mathcal{T} = \frac{1}{2}(m_Q + m_L)\dot{x}_L \cdot \dot{x}_L - m_Q L \dot{x}_L \cdot \dot{q} + \frac{1}{2} m_Q L^2 \dot{q} \cdot \dot{q} + \frac{1}{2} \Omega \cdot J \cdot \Omega \tag{2-19}$$

$$\mathcal{U} = (m_Q + m_L) g x_L \cdot e_3 - m_Q g L q \cdot e_3 \tag{2-20}$$

The variations of the $\mathcal{T}$ and $\mathcal{U}$ are approximated by a first-order Taylor approximation, which results in

$$\begin{aligned} \delta\mathcal{T} &\approx \frac{\partial \mathcal{T}}{\partial \dot{x}_L} \delta \dot{x}_L + \frac{\partial \mathcal{T}}{\partial \dot{q}} \delta \dot{q} + \frac{\partial \mathcal{T}}{\partial \Omega} \delta \Omega \\ &= ((m_Q + m_L)\dot{x}_L - m_Q L \dot{q}) \cdot \delta \dot{x}_L + (-m_Q L \dot{x}_L + m_Q L^2 \dot{q}) \cdot \delta \dot{q} + J\Omega \cdot \delta\Omega \end{aligned} \tag{2-21}$$

$$\begin{aligned} \delta\mathcal{U} &\approx \frac{\partial \mathcal{U}}{\partial x_L} \delta x_L + \frac{\partial \mathcal{U}}{\partial q} \delta q \\ &= (m_Q + m_L) g e_3 \cdot \delta x_L - m_Q g L e_3 \cdot \delta q \end{aligned} \tag{2-22}$$

The first term of virtual work is obtained from f acting on the QR and is given by the following term,

$$\begin{aligned} \delta W_1 &= f R e_3 \cdot \sum_{j=1}^{3} \frac{\partial x_Q}{\partial \mathbf{q}_j} \delta \mathbf{q}_j \\ &= f R e_3 \cdot (\delta x_L - L \delta q) \end{aligned} \tag{2-23}$$

where $\mathbf{q_j} = x_L, q, R$ and x_Q is substituted by Equation 2-10 The second term of virtual work is obtained from M acting on the QR. This gives the following term

$$\begin{aligned} \delta W_2 &= M \cdot \sum_{j=1}^{3} \frac{\partial \Omega}{\partial \dot{\mathbf{q}}_j} \delta \dot{\mathbf{q}}_j \\ &= M \cdot (R^T \delta R) \end{aligned} \tag{2-24}$$

The variations in energy and the virtual work can be substituted into Equation 2-15.

Equation 2-26 is a function of variations on manifolds, where δR is a variation on $SO(3)$ and δq is a variation on $\mathbb{S}^2$. The so called infinitesimal variations required to solve this equation are described as [14, 15]

$$\begin{aligned} \delta q &= \xi \times q \in T_q \mathbb{S}^2, \text{ where } \xi \in \mathbb{R}^3, \xi \cdot q = 0 \\ \delta \dot{q} &= \\ \delta R &= R\hat{\eta} \in T_R SO(3), \text{ where } \eta \in \mathbb{R}^3, \hat{\eta} \in \mathfrak{so}(3) \\ \delta \dot{R} &= \\ \delta \hat{\Omega} &= \end{aligned} \tag{2-25}$$

Substituting the variations in energy and the variations in

$$\begin{aligned} \delta S &= \int_{t_1}^{t_2} (\delta W_1 + \delta W_2 + \delta \mathcal{T} - \delta \mathcal{U}) dt \\ &= \\ &= \end{aligned} \tag{2-26}$$

The QR attitude kinematics equation is given by

$$\begin{aligned} \dot{x}_L &= \\ (m_Q + m_L)(\dot{v}_L + g e_3) &= \\ \dot{q} &= \\ m_Q L \dot{\omega} &= \\ \dot{R} &= R\hat{\Omega} \\ J\dot{\Omega} + \Omega \times J\Omega &= \end{aligned} \tag{2-27}$$

Summary

A Geometric Mechanics modeling approach is applied to represent the system dynamics on nonlinear configuration manifolds.

Geometric Mechanics allows a compact, unambiguous representation of the model dynamics.

In the next chapter nonlinear geometric control is discussed, which is based on the obtained nonlinear geometric representation of the model.

Chapter 3

Control Design

Section 3-1 introduces Nonlinear Geometric Control and the control design structure is discussed. Due to under-actuation, the load position tracking problem requires a backstepping control approach in order to control different flight modes.
In this section the tracking errors are defined on nonlinear manifolds, similar to the representation of the system dynamics.

The controllers that are designed for the control of the different flight modes, are discussed in Sections 3-2, 3-3 and 3-4.

3-1 Nonlinear Geometric Control

Many control systems are developed for the standard form of ordinary differential equations, namely $\dot{x} = f(x, u)$, where the state and the control input are denoted by x and u. It is assumed that the state and the control input lie in Euclidean spaces, and the system equations are defined in terms of smooth functions between Euclidean spaces. However, for many interesting mechanical systems, the configuration space cannot be expressed globally as a Euclidean space.

Geometric Control Theory is the study of how the geometry of the state space influences controls problems. In control systems engineering, the underlying geometric features of a dynamic system are often not considered carefully. Differential geometric control techniques utilize the geometric properties for control system design and analysis. The objective is to describe the system dynamics and control inputs on manifolds instead of local charts. In contrast to locally defined linear control, nonlinear geometric control can be defined almost globally, avoiding singularities that occur in the representation of large angles and complex maneuvering.

Attitude control systems naturally evolve on non-linear configurations such as $\mathbb{S}^2$ and $SO(3)$. Tracking control system can be developed on $SO(3)$, therefore it avoids singularities of Euler-Angles.

Global nonlinear dynamics of various classes of closed loop attitude control systems have been studied in recent years [**?**]. In contrast to hybrid control systems [16], complicated reachability set analysis is not required to guarantee safe switching between different flight modes, as the region of attraction for each flight mode covers the configuration space almost globally.

Backstepping Control A backstepping approach, or cascade control, is a Lyapunov based technique to design the control of nonlinear dynamical systems and ensuring Lyapunov stability. This approach is commonly used for the control of QRs [17] and will also be used in this research for the control of the load trajectory tracking problem. The principle is to create a cascaded structure by starting with a stable system as a base, then "stepping back" from this base to add a control loop around it that stabilizes the added subsystem to enable the control of another state. This is repeated until the final external control is reached. The control law is designed by using states as virtual control signals. Each loop computes a virtual command signal, denoted by subscript c, as a tracking command for the inner loops.

Because the QR has only four actuators, it is not possible to control all DOFs of the QR-Load system simultaneously. The backstepping approach allows control of different flight modes in which parts of the DOFs are controlled. The flight modes and their functions are defined as follows

- QR Attitude Controlled Mode
  - Track a desired QR attitude $R_d(t)$ and a heading direction $b_{1_d}(t)$
  - Give a desired input M for system
- Load Attitude Controlled Mode
  - Track a desired load attitude command $q_d(t)$
  - Give a computed QR attitude R_c for the QR attitude controller (instead of $R_d(t)$)
- Load Position Controlled Mode
  - Track a desired load position $x_{L,d}(t)$
  - Give a computed load attitude q_c for the load attitude controller (instead of $qR_d(t)$)

where the subscript $\cdot_d$ denotes a desired tracking reference, and $\cdot_c$ denotes a computed value that is calculated as a tracking reference.

The controller that is used in this research is shown in Figure 3-1. The lowest levels have the highest bandwidth and are in control of the rotor rotational speeds ω_i, the total force f and moments M. The next level controls the load attitude q, and the top level controls the load position x_L.

The design of the controllers for the QR attitude can be found in [3] and for the load attitude- and position this can be found in [15]. Thorough stability analyses are presented in either references. For a deeper understanding of Lyapunov stability analysis in geometric control, the reader can refer to [14].

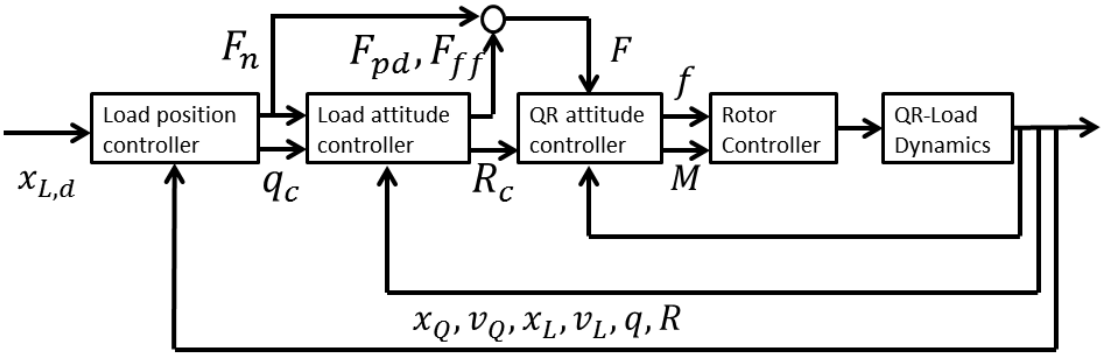

Figure 3-1: Nonlinear Geometric Control Loop of the QR-Load system

Configuration Errors The system dynamics evolve on nonlinear manifolds, that describe the configuration spaces for the QR attitude $\in SO(3)$ and the load attitude $\in \mathbb{S}^2$. Likewise, configuration errors can be described on these manifolds. The derivation of the attitude and velocity errors can be found in [14].

The attitude error is denoted as $R_d^T R$, and it describes the relative rotation from the body frame to the desired frame. The QR attitude error function on $SO(3)$ is chosen to be

$$\Psi_R(R, R_d) = \frac{1}{2} tr\left[I - R_d^T R\right] \tag{3-1}$$

Ψ_R is locally positive-definite about $R_d^T R = I$ within the region where the rotation angle between R and R_d is less than 180°. It can be shown that this region where $\Psi_R < 2$ almost covers $SO(3)$. The derivative of Equation 3-1 is given by

$$\mathbf{D}_R \Psi(R, R_d) \cdot R\hat{\eta} = \frac{1}{2}(R_d^T R - R^T R_d)^\vee \cdot \eta \tag{3-2}$$

where the *vee map* $^\vee : \mathfrak{so}(3) \to \mathbb{R}^3$ is the inverse of the *hat map* defined in Section 2-1. From this, the attitude tracking error is chosen to be

$$e_R = \frac{1}{2}(R_d^T R - R^T R_d)^\vee \tag{3-3}$$

The tangent vectors $\dot{R}$ and $\dot{R}_d$ cannot be compared directly, since they do not lie in the same space. They each are defined in their own tangent spaces, denoted by $\dot{R} \in T_R SO(3)$ and $\dot{R}_d \in T_{R_d} SO(3)$. $\dot{R}_d$ is transformed into a vector on $T_R SO(3)$ to compare it with $\dot{R}$. This can be done by an mathematical object called a *transport map*, that enables the comparison of tangent vectors living in different spaces.

The velocity error that corresponds to the transport map is defined as

$$\dot{e} = \dot{R} - \dot{R}_d(R_d^T R) \tag{3-4}$$

Substituting Equations 2-1 and 2-2, $\dot{R}_d$ can now be compared with $\dot{R}$ through

$$\begin{aligned}\dot{R} - \dot{R}_d(R_d^T R) &= R\hat{\Omega} - R_d\hat{\Omega}_d(R_d^T R) \\ &= R(\Omega)^\wedge - (RR^T)R_d\hat{\Omega}_d R_d^T R \\ &= R(\Omega)^\wedge - R(R^T R_d\Omega_d)^\wedge \\ &= R(\Omega - R^T R_d\Omega_d)^\wedge\end{aligned} \tag{3-5}$$

The velocity tracking error in $\{\mathcal{B}\}$ can now be defined as

$$e_\Omega = \Omega - R^T R_d\Omega_d \tag{3-6}$$

The load attitude error function on $\mathbb{S}^2$ is chosen to be

$$\Psi_q = 1 - q_d^T q \tag{3-7}$$

In the same fashion a *transport map* is used for a comparison between the tangent spaces $T_q\mathbb{S}^2$ and $T_{q_d}\mathbb{S}^2$. This results in the following error functions on $T\mathbb{S}^2$

$$e_q = \hat{q}^2 q_d \tag{3-8}$$
$$e_{\dot{q}} = \dot{q} - (q_d \times \dot{q}_d) \times q \tag{3-9}$$

The tracking errors for position and velocity are defined as

$$e_x = x - x_d \tag{3-10}$$
$$e_v = v - v_d \tag{3-11}$$

where $v_d = \dot{x}_d$ and $x_d(t) \in \mathbb{R}^3$ is a smooth desired load position.

3-2 Quadrotor Attitude Tracking

QR Attitude Controlled Mode is designed to control the QR attitude by tracking a desired QR attitude command $R_d(t)$ and a heading direction $b_{1_d}(t)$.

The calculation of the moment consists of a proportional term, a derivative term and a canceling term, and is defined as follows [3]

$$M = \frac{1}{\epsilon^2}k_R e_R - \frac{1}{\epsilon}k_\Omega e_\Omega + \Omega \times J\Omega - J(\hat{\Omega}R^T R_d\Omega_d - R^T R_d\dot{\Omega}_d) \tag{3-12}$$

for any positive constants k_R, k_Ω, and $0 < \epsilon < 1$. Where ϵ is a parameter to enable rapid exponential convergence of the attitude error functions. $\dot{\Omega}_d$ follows from

$$\begin{aligned}\dot{R}_d &= R_d\hat{\Omega}_d \\ \hat{\Omega}_d &= R_d^T\dot{R}_d\end{aligned} \tag{3-13}$$

$$\begin{aligned}\dot{\hat{\Omega}}_d &= (\dot{R}_d^T \dot{R}_d) + (R_d^T \ddot{R}_d) \\ &= (R_d \hat{\Omega}_d)^T (R_d \hat{\Omega}_d) + (R_d^T \ddot{R}_d) \\ &= -\hat{\Omega}_d \hat{\Omega}_d + R_d^T \ddot{R}_d, \\ \hat{\Omega}_d &= (-\hat{\Omega}_d \hat{\Omega}_d + R_d^T \ddot{R}_d)^\vee\end{aligned} \tag{3-14}$$

It is proven in [3] that the zero equilibrium of the closed loop tracking error $(e_R, e_\Omega) = (0, 0)$ is exponentially stable, if the initial conditions satisfy

$$\Psi_R(R(0), R_d(0)) < 2 \tag{3-15}$$

$$\| e_\Omega(0) \|^2 < \frac{2}{\lambda_M(J)} \frac{k_R}{\epsilon^2} (2 - \Psi_R(R(0), R_d(0))) \tag{3-16}$$

where $\lambda_M(\cdot)$ denotes the maximum eigenvalue.

Furthermore, there exist constants $\alpha_R, \beta_R > 0$ such that

$$\Psi_R(R(t), R_d(t)) \leq min \left\{ 2, \alpha_R e^{-\beta_R t} \right\} \tag{3-17}$$

The domain of attraction is defined by Equations 3-15 and 3-16. [3] shows the derivation of a stability analysis of the controller is presented.

3-3 Load Attitude Tracking

The Load Attitude Controlled Mode tracks a desired load attitude q_d by calculating a command signal for the QR attitude, defined as

$$R_c = \left[b_{1c}; b_{3c} \times b_{1c}; b_{3c} \right] \tag{3-18}$$

where $b_{3c} \in \mathbb{S}^2$ is defined by

$$b_{3c} = \frac{F}{||F||} \tag{3-19}$$

Such that F in Equation 3-19 is defined by a normal component F_n, F_{pd} and F_{ff}

$$F = F_n - F_{pd} - F_{ff} \tag{3-20}$$

Control forces for a system evolving on $\mathbb{S}^2$, are derived in [14]. This results in a proportional-derivative force F_{pd} and a feed forward force F_{ff}, that are functions of Equations 3-8 and 3-9. The following terms are obtained

$$\begin{aligned}F_{pd} &= -k_P \hat{q}^2 q_d - k_D (\dot{q} - (q_d \times \dot{q}_d \times q) \\ &= -k_q e_q - k_\omega e_{\dot{q}}\end{aligned} \tag{3-21}$$

$$F_{ff} = m_Q L \langle \langle q, q_d \times \dot{q}_d \rangle \rangle_{\mathbb{R}^3} (q \times \dot{q}) + m_Q L (q_d \times \ddot{q}_d) \times q \tag{3-22}$$

The unit vector b_{1c} is defined as

$$b_{1c} = -\frac{1}{||b_{3c} \times b_{1d}||}(b_{3c} \times (b_{3c} \times b_{1d})) \tag{3-23}$$

where $b_{1d} \in \mathbb{S}^2$ is chosen, not parallel to b_{3c}. The total upward thrust is defined as

$$f = F \cdot Re_3 \tag{3-24}$$

It is proven in [15] that the zero equilibrium of the closed loop tracking error $(e_q, e_{\dot{q}}, e_R, e_\Omega) = (0, 0, 0, 0)$ is exponentially stable, if the initial conditions satisfy

$$\Psi_q(q(0), q_d(0)) < 2 \tag{3-25}$$

$$\| e_{\dot{q}}(0) \|^2 < \frac{2}{m_Q L} k_R (2 - \Psi_q(q(0), q_d(0))) \tag{3-26}$$

The domain of attraction is defined by Equations 3-15, 3-16, 3-25 and 3-26. Furthermore, there exist constants $\alpha_q, \beta_q > 0$ such that

$$\Psi_q(q(t), q_d(t)) \leq min \left\{ 2, \alpha_q e^{-\beta_q t} \right\} \tag{3-27}$$

3-4 Load Position Tracking

Tracks load position reference. Outputs load attitude reference.

$$q_c = -\frac{A}{||A||} \tag{3-28}$$

where

$$A = -k_x e_x - k_v e_v + (m_Q + m_L)(\ddot{x}_{L,d} + g e_3) + m_Q L (\dot{q} \cdot \dot{q}) q \tag{3-29}$$

with $e_x = x_L - x_{L,d}$ and $e_v = \dot{x}_L - \dot{x}_{L,d}$. Furthermore, F_n is redefined as

$$F_n = (A \cdot q) q \tag{3-30}$$

It is proven in [15] that the zero equilibrium of the closed loop tracking error $(e_x, e_v, e_q, e_{\dot{q}}, e_R, e_\Omega) = (0, 0, 0, 0, 0, 0)$ is exponentially stable, if the initial conditions satisfy

$$\Psi_q(q(0), q_c(0)) < \psi_1 < 1 \tag{3-31}$$

$$\| e_x(0) \|^2 < e_{x_{max}} \tag{3-32}$$

where $e_{x_{max}}$ and ψ_1 are fixed constants.

The domain of attraction is defined by Equations 3-15, 3-16, 3-31 and the following equation

$$\| e_{\dot{q}}(0) \|^2 < \frac{2}{m_Q L} k_q (\psi_1 - \Psi_q(q(0), q_d(0))) \tag{3-33}$$

Furthermore, there exist constants $\alpha_q, \beta_q > 0$ such that

$$\Psi_q(q(t), q_d(t)) \leq min \left\{ 2, \alpha_q e^{-\beta_q t} \right\} \tag{3-34}$$

3-5 Stability Analysis

Lyapunov Analysis on SO3 x R3 and S2 x R3 Closed-loop full-attitude dynamics evolve on the non- Euclidean manifold SO3 x R3. Since these manifolds are locally Euclidean, local stability properties of a closed-loop equilibrium solution can be assessed using standard Lyapunov methods. In addition, the LaSalle invariance result and related Lyapunov results apply to closed-loop vector fields defined on these manifolds. However, since the manifolds SO3 and S2 are compact, the radial unboundedness assumption cannot be satisfied; consequently, global asymptotic stability cannot follow from a Lyapunov analysis on Euclidean spaces [40], and therefore must be analyzed in alternative ways [19]–[23].[8, p.43]

[8] summarizes global results on attitude control and stabilization for a rigid body using continuous time- invariant feedback. The analysis uses methods of geometric mechanics based on the geometry of the special orthogonal group SO3 and the two-sphere S2.

Summary

In this chapter the control design based on Nonlinear Geometric Control was discussed.

The main difference with other control techniques is that the tracking errors are also defined on manifolds, which allows the design of almost global defined controllers.

Stability analysis is different from a Lyapunov analysis on Euclidean spaces.

In order to test the control performance of a load position tracking objective, experiments are defined in the next chapter.

Chapter 4

Experiment

The experimental procedure is explained in Section 4-1. It is discussed what experiments can be done in order to investigate the possibilities of nonlinear geometric control. In addition a comparison will be made between the performances of the Nonlinear Geometric Controller and a linear LQR controller.

The controllers are tested on their ability to track a desired load trajectory. Section 4-2 presents trajectories that create situations with different challenges. It is discussed what could be expected from these experiments, and in what way a comparison can be made between the performance of the controllers.

In Section 4-3 the experimental setup is discussed. The model parameters for the QR-Load system are presented, as well as the controller parameters for both nonlinear Geometric controller and LQR controller. The notion of a backstepping command filter is made to illustrate its use in the experiments.

4-1 Procedure

Performance of both LQR control and a Nonlinear Geometric Control could be evaluated by comparing their ability to track a load trajectory with minimal error. However, in linear control small angles of both load and QR are assumed. As a result, the linearized model does not allow direct reference tracking of the load position. The LQR cost function allows control of the inputs f and M, and the states which define the QR position, QR attitude and load attitude. Therefore, load control is only possible by minimizing the load swing. This fact illustrates an important difference between the use of a linear and a nonlinear model.

The experiments describe a desired load trajectory $x_{L,d}(t)$, which is required to be smooth for Geometric Control, such that feed forward terms can be generated and implemented. In this thesis the desired load paths are generated by hand, and the required velocity and acceleration is calculated by a command filter, of which the details are described in Section 4-3.

The experiments done with the LQR controller will apply reference tracking of the QR position, which is based on the desired load trajectories that are used for the nonlinear Geometric controller. When assuming small angles and minimal load swing, the QR position is approximately a cable length above the predefined desired load position. Note that this will not allow a direct comparison of the load trajectory tracking, nevertheless this will illustrate the main differences between the controllers with the same purpose of load transportation, but with a different approach.

4-2 Trajectories

What observations can be made in order to adapt the controller properties that improve performance of the test cases. Description of tests that apply on all cases.

4-2-1 Case A

In this case a smooth step-like trajectory is generated to transport the load from a starting position along the direction of the x-asis to the final position. In a regular step function the system is subjected to a sudden input. The stability of the system can be investigated by observing whether it is able to reach a stationary final state, and how fast this can be reached. It can be seen whether the system responds with an overshoot and how fast the response is, when the controller tries to track the trajectory.

Figure 4-1 shows the desired trajectory over time, and a three dimensional representation.

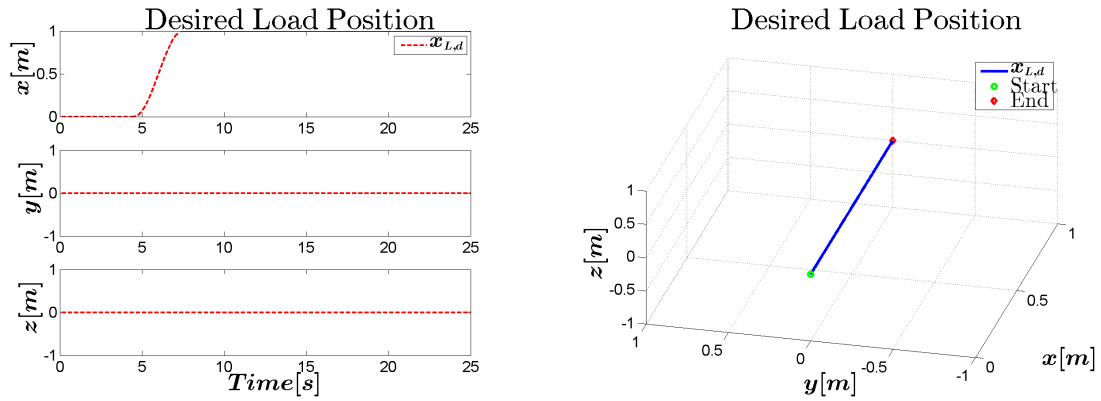

(a) (b)

Figure 4-1: Desired Load Position Case A

4-2-2 Case B

PLANNING: make case to test limits on QR angles while tracking load trajectory. Is nonlinear GC useful for such aggressive maneuvers?

4-2-3 Case C

For this case a trajectory is generated to test multiple disciplines. The trajectory has the shape of a sine wave that moves along the y-axis and varies in amplitude in the direction of the x-axis, while going up and down in the direction of the z-axis. The changing amplitude of the trajectory that moves from side to side, requires varying velocities to 'keep up' with the trajectory. It can be expected that the nonlinear geometric control allows large QR angles, whereas the LQR will possible fail to deviate far from the equilibrium point.

Figure 4-2 shows the desired trajectory over time, and a three dimensional representation.

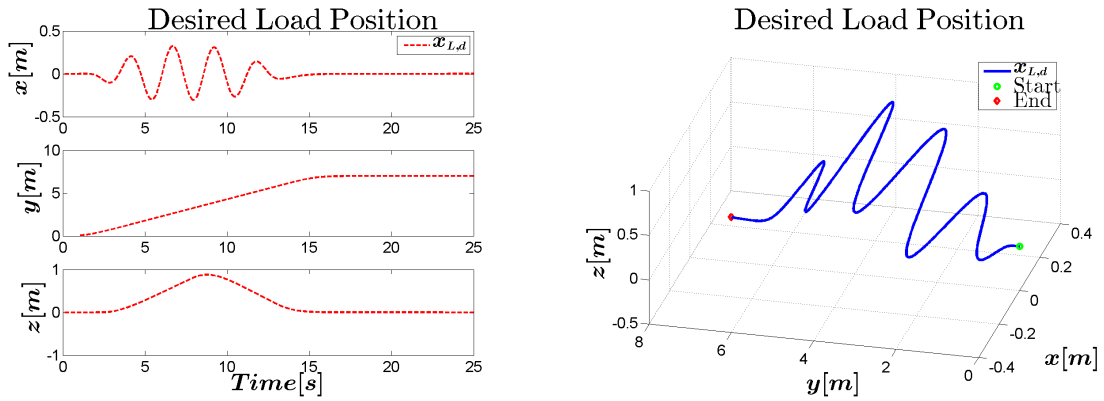

(a) (b)

Figure 4-2: Desired Load Position Case C

4-3 Setup

Model parameters The simulations are developed using Matlab and Simulink, using the system parameters found in Table 4-1.

Parameter	Value		Description
m_Q	4.34	kg	Quadrotor Mass
m_L	0.1	kg	Load Mass
l	0.315	m	Arm length from QR CoM to rotor
L	0.7	m	Cable Length
I_{xx}	0.0820	kgm^2	Quadrotor Inertia about x-axis
I_{yy}	0.0845	kgm^2	Quadrotor Inertia about y-axis
I_{zz}	0.1377	kgm^2	Quadrotor Inertia about z-axis
d			Drag Constant
b			Thrust Constant
c_{τ_f}			Constant

Table 4-1: Modeling Parameters

LQR Control Linear Quadratic Regulator (LQR) control uses an algorithm to obtain a state-feedback controller, minimizing a cost function depending on the states and weight factors. An LQR design is shown in Figure 4-3

Figure 4-3: LQR control design

LQR control is based on a small angle assumption. Therefore, a traditional modeling method may represent the rotation matrix with a local coordinate system, for example with an Euler Angle parameterization. A continuous time linearized model of the system used in this controller is represented in the following form

$$\dot{\mathbf{x}} = A\mathbf{x} + Bu \tag{4-1}$$
$$y = C\mathbf{x} + Du \tag{4-2}$$

where $\mathbf{x}$ is the state vector and u is the input vector, defined as follows

$$\mathbf{x} = \begin{bmatrix} x & y & z & \phi & \theta & \psi & \phi_L & \theta_L & \dot{x} & \dot{y} & \dot{z} & \dot{\phi} & \dot{\theta} & \dot{\psi} & \dot{\phi}_L & \dot{\theta}_L \end{bmatrix}^T \tag{4-3}$$
$$u = \begin{bmatrix} f & M_\phi & M_\theta & M_\psi \end{bmatrix}^T \tag{4-4}$$

where ϕ_L and θ_L are the angle of rotation of the load about the x-axis and y-axis in $\{\mathcal{B}\}$, respectively. The derivation of A, B, C, D can be found in Section A-2.

Using `Matlab` command `lqr(A,B,Q,R)`, an optimal gain matrix K is calculated, such that the state-feedback law $u = -K\mathbf{x}$ minimizes the quadratic cost function defined as

$$J(u) = \int_0^\infty (\mathbf{x}^T Q\mathbf{x} + u^T Ru)dt \tag{4-5}$$

The weight matrices Q and R that define the effects of the states and inputs in the cost function, and the calculated gain matrix K can be found in Section A-2.

Geometric Control The chosen controller gains in Equations 3-12,3-18,3-28 can be found in Table 4-2.

Command Filtering A consequence of a backstepping control approach, is that it also increases the order of the states. The inner control loops become a function of the commanded signals and their higher derivatives, which are generated by an outer loop. In the earlier presented control design, the load attitude controller generates a commanded QR attitude R_c and its derivative $\dot{R}_c$. In the same fashion, the load position controller generates a commanded load attitude q_c and its derivative $\dot{q}_c$. Instead of analytic differentiation of these terms, which can be tedious and require high computational costs, these values can be obtained with the use of a Command Filter, which is explained in more detail in [18].

Gain	Value
k_R	
k_Ω	
k_q	
k_ω	
k_x	
k_v	

Table 4-2: Controller Gains

The basic idea is that the command signal is pre-filtered by a low pass filter and generates an estimation of the derivatives of the commanded signal. In this thesis a backstepping command filter of third order is applied to compute $\dot{R}_c, \ddot{R}_c, \dot{q}_c, \ddot{q}_c$. The transfer function of the original commanded input signal X_c^o and the filtered output X_c has the form

$$\frac{X_c(s)}{X_c^o(s)} = H(s) = \frac{\omega_{n1}}{s+\omega_{n1}} \cdot \frac{\omega_{n2}^2}{s^2 + 2\zeta\omega_{n2}s + \omega_{n2}^2} \tag{4-6}$$

Where ζ is the damping ratio and ω_n the undamped natural frequency. See Figure **??** and A-2. The filter has the following state space representation

$$\dot{x}_1 = x_2 \tag{4-7}$$
$$\dot{x}_2 = x_3 \tag{4-8}$$
$$\dot{x}_3 = -(2\zeta\omega_{n2} + \omega_{n1})x_3 - (2\zeta\omega_{n1}\omega_{n2} + \omega_{n2}^2)x_2 - (\omega_{n1}\omega_{n2}^2)(x_1 - x_c^o) \tag{4-9}$$

where $x_1 = x_c$, $x_2 = \dot{x}_c$ and $x_3 = \ddot{x}_c$.

Chapter 5

Results

The sections in this chapter discuss the results that are obtained from the load trajectory tracking experiments.

In Figures 5-2, 5-4 and 5-6 the load tracking performance is shown for the Nonlinear Geometric Controller. From these figures the tracking errors of the QR attitude, load attitude and load position, and the stability of the tracking errors can be analyzed.

5-1 Case A

Figure 5-1a shows the load position along the desired load position $x_{L,d}$ for both control approaches.
Figure 5-1b shows the load position error for both control approaches.

Figure 5-1c shows the QR attitude with respect to $\{\mathcal{I}\}$.
In Figure 5-1d the load angle with respect to $\{\mathcal{B}\}$ is shown.
Observations:

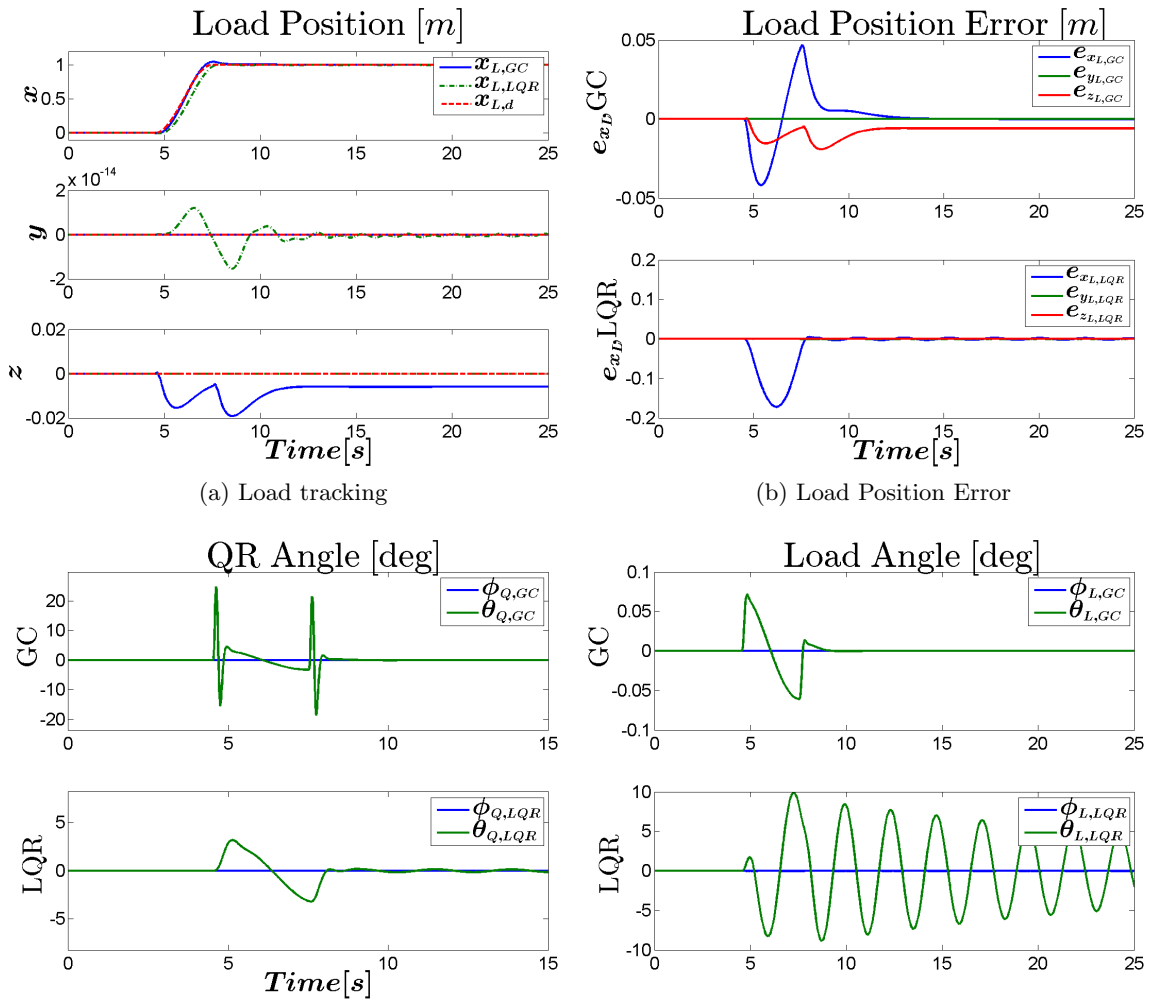

(a) Load tracking

(b) Load Position Error

(c) QR Attitude

(d) Load Attitude

Figure 5-1: Controller Comparison Case A

The desired and actual load trajectory, and the position error are shown in Figure 5-2a and Figure 5-2b, respectively. From this can be seen that a small steady state error remains in the z-direction. However, $(e_x, e_v) = (0, 0)$ is exponentially attractive.

Figure 5-2c and 5-2d show the tracking errors of the QR attitude and load attitude, respectively.

Observations: $(e_x, e_v, e_q, e_{\dot{q}}, e_R, e_\Omega) = (0, 0, 0, 0, 0, 0)$ is exponentially stable

Figure 5-2e and 5-2f show the tracking error functions of the QR and load, respectively. Observations: there exist constants $\alpha_q, \beta_q > 0$ such that

$$\Psi_q(q(t), q_d(t)) \leq min\left\{2, \alpha_q e^{-\beta_q t}\right\} \tag{5-1}$$

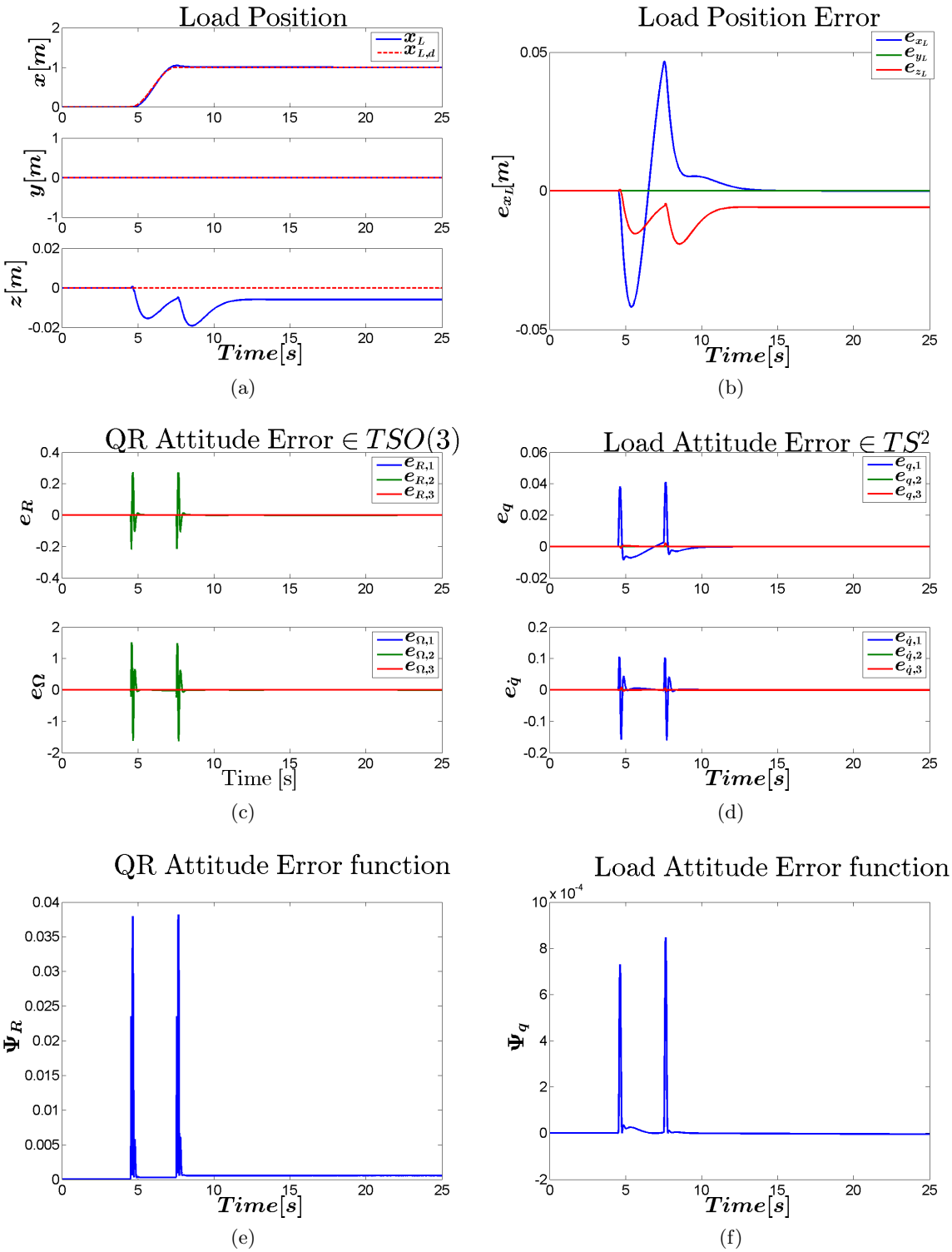

Figure 5-2: Results Nonlinear Geometric Control Case A

5-2 Case B

Figure 5-3a shows the load position along the desired load position $x_{L,d}$ of both controllers.

(a) Load tracking (b) Load Position Error

Figure 5-3: Controller Comparison Case B

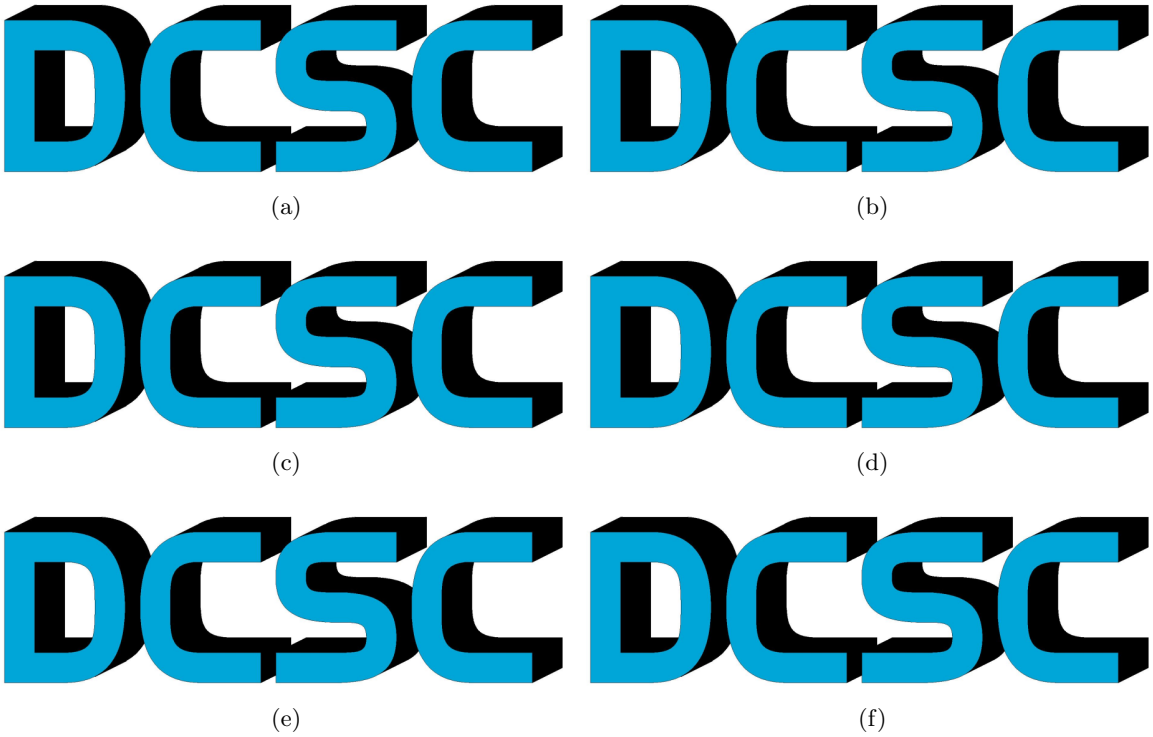

(a) (b)

(c) (d)

(e) (f)

Figure 5-4: Results Nonlinear Geometric Control Case B

5-3 Case C

Figure 5-5a shows the load position along the desired load position $x_{L,d}$ of both controllers.
Figure 5-5b shows the load position error for both control approaches.
Observations: fact that LQR can not control load position is obvious.
OTHER GAINS FOR LQR!
Very small penalty on load angle results in swinging load; decreasing load position error, but very bad anti-swing.

Figure 5-5c shows the QR attitude with respect to $\{\mathcal{I}\}$.
In Figure 5-5d the load angle with respect to $\{\mathcal{B}\}$ is shown.
Observations: Load angles are huge, check results

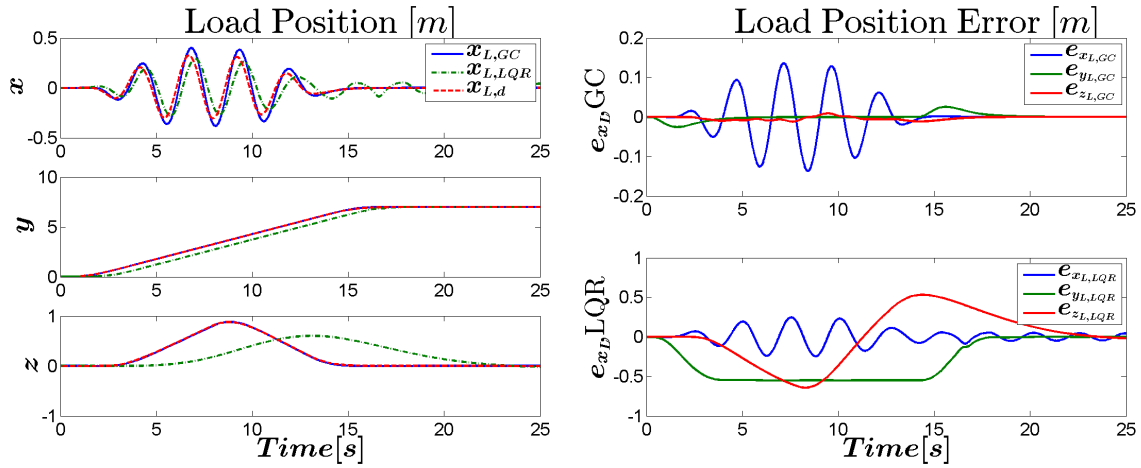

(a) Load tracking

(b) Load Position Error

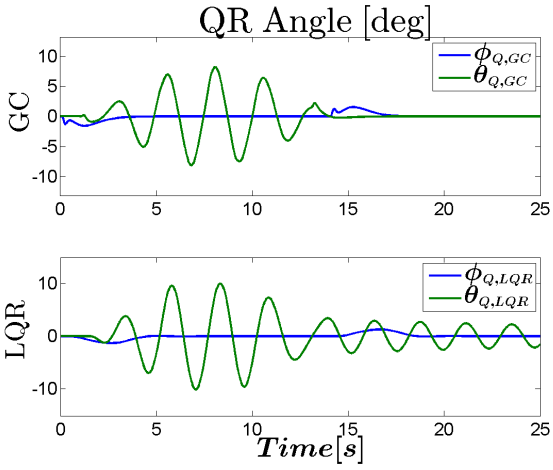

(c) QR Attitude

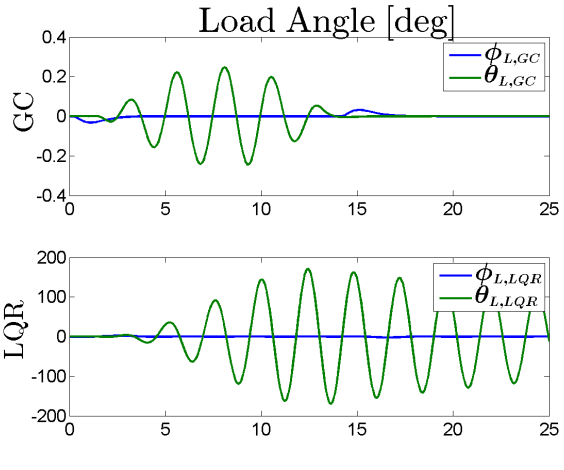

(d) Load Attitude

Figure 5-5: Controller Comparison Case C

While tracking the required QR attitude, which tilts the QR to reach the desired velocities in the right direction, it can be seen that the system has difficulties to also maintain the desired

height, which can be explained by the fact that the total force will not point upwards if the QR is tilted. Despite the fact that the QR is moving from side to side, the upward force is still controlled to track the desired height.

Figure 5-6a shows the desired load position, and Figure 5-6b shows that the error is mainly the overshoot in the x-direction, due to the fast desired swinging motion.

Figure 5-6c and 5-6d show the tracking errors of the QR attitude and load attitude, respectively.
Observations: $(e_x, e_v, e_q, e_{\dot{q}}, e_R, e_\Omega) = (0, 0, 0, 0, 0, 0)$ is exponentially stable

Figure 5-6e and 5-6f show the tracking error functions of the QR and load, respectively.
Observations: there exist constants $\alpha_q, \beta_q > 0$ such that

$$\Psi_q(q(t), q_d(t)) \leq min\left\{2, \alpha_q e^{-\beta_q t}\right\} \tag{5-2}$$

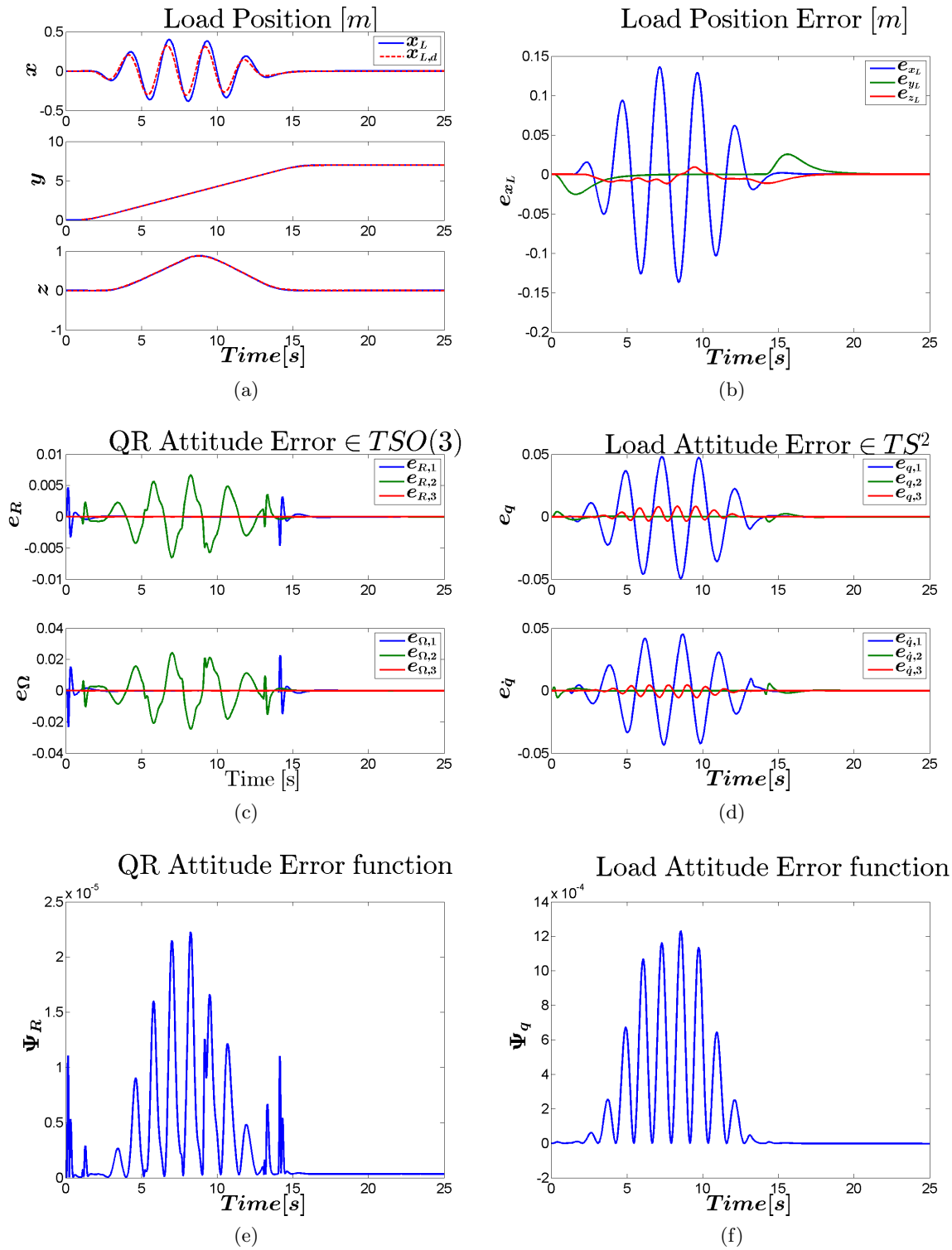

Figure 5-6: Results Nonlinear Geometric Control Case C

5-4 Conclusion

Near the equilibrium configuration, the LQR controller is able to reduce the swing.

The nonlinear geometric controller depends on feed forward terms that are obtained from the desired trajectories. Trajectory generation approaches exist that are able to generate the required desired position, velocity and acceleration by however it is possible to compute these with trajectory generating algorithms too.

The controllers are functions of the computed tracking references q_c, R_c and their derivatives. These terms are approximated by a command filter, which means that the accuracy decreases because high frequency terms are filtered.

Chapter 6

Conclusions and Future Work

6-1 Summary and Conclusions

This report starts by introducing the subject. The aim is described and the motivation for this research is given.

After the main introduction, the concepts of Geometric Mechanics are introduced. Instead of the trivial Euclidean spaces defined by Cartesian coordinates, the configuration space of the model is described on nonlinear manifolds. This approach is used to obtain a model through the tools of Differential Geometry.

Based on the geometric model, a nonlinear geometric control design is discussed. A back-stepping approach, allows different DOFs of the under-actuated system to be controlled in a cascaded structure. The geometric control is based on are functions of error functions defined on nonlinear manifolds. by Differential Geometry.

Next, the experiment is defined. The nonlinear controller is used to track desired load trajectories in different situations. The nonlinear performance is compared to an LQR control Testing the nonlinear Geometric Controller To compare with a common linear controller, LQR control is used to compare Results are,

The conclusions that can be extracted from the experiments is that

6-2 Recommendations for Future Work

6-2-1 Investigate Implementation

Digital Control The concept of Geometric Control is shown under the assumption of continuous-time control. However, an analysis must be done in the discrete-time domain for the implementation of a real-time application. This must verify whether it is feasible to run the controller on an on-board processor on a QR. The control performance could be limited by the bandwidth of either the discretized control system or the wireless communication.

It must be investigated whether the control system is still able to deal with the fast dynamics that are required for aggressive maneuvering. Continuous-time Euler-Lagrange equations could be found by minimizing the action integral, which is a function of the Lagrangian. In a similar procedure the discrete-time Euler-Lagrange can be obtained, by minimizing te summation of a discrete Lagrangian, which is demonstrated in [10].

Model identification and validation In this thesis the model parameters are either obtained from examples in literature or arbitrarily chosen. In practice, identification and validation of the QR model and rotor dynamics is required. The mathematical model requires inclusion of the masses, inertia matrix and lengths of the QR, as well as the drag and thrust constants of the rotors, that are very unlikely to be identical.

As a theoretical extension the influence of model mismatches could be simulated.

Robustness The control in this thesis assumes perfect state feedback. In practice the controller depends on visual feedback or data obtained from an on-board inertial measurement unit. Unlike in simulations, this data will contain noise, uncertainties and possibly drift. Based on a nonlinear geometric approach for a QR without load, [4] includes uncertainties in the translational dynamics and rotational dynamics to prove the robustness against unstructured uncertainties. This work could be extended to a QR-Load system to investigate the effects of non-perfect state feedback.

Due to uncertainties In what way would parameter choice in the controllers affect robustness? To test the controller for

How to estimate states?

Parameter Estimation can be done by

State Estimation can be done by

Drawback: assumes all states to be known

Model based. What if analytical model is not accurate?

What parameters must be

6-2-2 Minimum Snap Trajectory Generation

The trajectories described in Section 4-2 were arbitrarily generated by hand to test the performance of the controller in different situations. Whenever more complex trajectories are desired, or when an optimal trajectory is required, this approach is no longer efficient and too complex to solve by hand. A recommended extension to this thesis is the automatic generation of a trajectory. This can be done as presented by [19] and applied in [7, 20], where a QP problem is solved by minimizing the second derivative of the acceleration (snap), guaranteeing a smooth optimal trajectory. The QP allows inclusion of input constraints and other requirements. It is proven that the system is *differential flat*, meaning that all states

and inputs can be expressed in terms of only four states and their derivatives. This property is used to transform the high-dimensional optimization problem into a four-dimensional problem.

6-2-3 Hybrid System

This thesis is only focused on the subsystem where the tension in the cable is non-zero. A possible extension is to apply hybrid control, such that the controller is able to switch between two subsystem models whenever the cable tension switches between zero and non-zero. A trajectory generation method that accounts for the switching dynamics of the hybrid system is presented in [7].

Appendix A

Appendix

A-1 Derivation of Equations of motion

A-1-1 Load Dynamics

Let x_{CM} denote the position of the center of mass of the combined Quadrotor-Load system, expressed in $\{\mathcal{I}\}$. Which can be found by

$$\begin{aligned} m_Q(x_Q - x_{CM}) + m_L(x_L - x_{CM}) &= 0 \\ (m_Q + m_L)x_{CM} &= m_Q x_Q + m_L x_L \end{aligned} \tag{A-1}$$

Applying Newton's laws of motion to (A-1) and inserting (2-10) gives the

$$\begin{aligned} (m_Q + m_L)\ddot{x}_{CM} &= fRe_3 - (m_Q + m_L)ge_3 \\ (m_Q + m_L)(\ddot{x}_L + ge_3) &= fRe_3 + m_Q L\ddot{q} \end{aligned} \tag{A-2}$$

Here comes the derivation of $\ddot{q}$, obtained by geometric mechanics.

A-2 LQR controller

A-2-1 Modeling

The linearized model is written into a first order ODE of the form

$$\dot{\mathbf{x}} = A\mathbf{x} + Bu \tag{A-3}$$

$$y = C\mathbf{x} + Du \tag{A-4}$$

with the following state- and input vectors

$$\begin{aligned} \mathbf{x} &= \begin{bmatrix} x & y & z & \phi & \theta & \psi & \phi_L & \theta_L & \dot{x} & \dot{y} & \dot{z} & \dot{\phi} & \dot{\theta} & \dot{\psi} & \dot{\phi}_L & \dot{\theta}_L \end{bmatrix}^T \\ u &= \begin{bmatrix} f & M_\phi & M_\theta & M_\psi \end{bmatrix}^T \end{aligned} \tag{A-5}$$

The model is linearized about the hovering flight mode. All translational and rotational velocities are zero during hover. The positional states and the yaw angle do not affect the dynamics, and are set equal to zero. A thrust input $u_1 = g(mQ+mL)$ is required to maintain hover, and all other control inputs are set equal to zero. The states and inputs in the equations of motion are substituted by an initial condition and a perturbation

$$\dot{\mathbf{x}} \to \dot{\mathbf{x}}_0 + \delta\dot{\mathbf{x}}, \quad \mathbf{x} \to \mathbf{x}_0 + \delta\mathbf{x}, \quad u \to u_0 + \delta u \tag{A-6}$$

$$\begin{aligned} \mathbf{x}(0) &= \mathbf{0} \\ u(0) &= \begin{bmatrix} g(m_Q + m_L) & 0 & 0 & 0 \end{bmatrix}^T \end{aligned} \tag{A-7}$$

The linearized equations of motion are rearranged into Equation A-8 and substituted in Equation A-3.

$$[content...] \begin{bmatrix} \delta\ddot{x} \\ \delta\ddot{y} \\ \delta\ddot{z} \\ \delta\ddot{\phi} \\ \delta\ddot{\theta} \\ \delta\ddot{\psi} \\ \delta\ddot{\phi}_L \\ \delta\ddot{\theta}_L \end{bmatrix} + [content...] \begin{bmatrix} \delta x \\ \delta y \\ \delta z \\ \delta\phi \\ \delta\theta \\ \delta\psi \\ \delta\phi_L \\ \delta\theta_L \end{bmatrix} = [content...] \begin{bmatrix} \delta u_1 \\ \delta u_2 \\ \delta u_3 \\ \delta u_4 \end{bmatrix} \tag{A-8}$$

```
1 LQRA =
```

```
  LQRB =
```

The tuning parameters of the LQR controller a chosen as follows

$$\begin{aligned} Q &= diag\begin{pmatrix} 10 & 10 & 100, & 1 & 1 & 1, & 1 & 1, & 1 & 1 & 1, & 1 & 1 & 1, & 1 & 1 \end{pmatrix} \\ R &= diag\begin{pmatrix} 0.044, & 1.56, & 1.56, & 1.56 \end{pmatrix} \end{aligned} \tag{A-9}$$

`Matlab` command `lqr(LQRA,LQRB,Q,R)` generates the following gain matrix K

```
  K =
```

A-3 Classical Modeling

This section describes the derivation of the model by using classical modeling techniques.

When assuming small angle maneuvers, *Euler-angles* can be used to locally parameterize the orientation of the body-fixed reference coordinate frame with respect to the inertial reference coordinate frame. Simple linear controllers are often based on a linearized dynamical model, applying this small angles assumption.

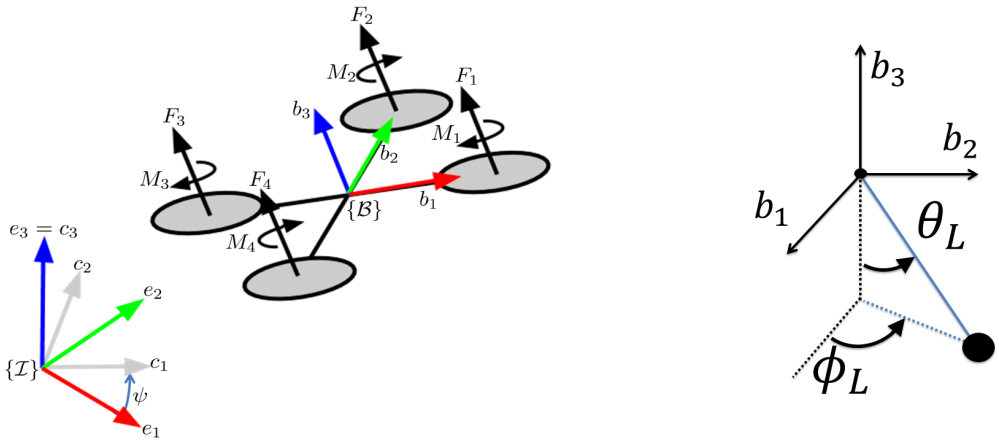

(a) Quadrotor model representation

(b) Load angles

Figure A-1: Model representation

The following equations of motion follow from Newton's law.

$$\begin{aligned} \dot{x}_Q &= v_Q \\ m_Q \dot{v}_Q &= fRe_3 - m_Q g e_3 - Tq \\ \dot{x}_L &= v_L \\ m_L \dot{v}_L &= -m_L g e_3 + Tq \end{aligned} \tag{A-10}$$

where $x_Q = x_L - Lq$. T is the cable tension, defined by $T = |f|q$, where $|f| = m_L \dot{v}_L$ is the magnitude of the force.

Because Euler-Angles are used, a function is required that maps a vector of the Z-X-Y Euler angles to its rotation matrix $R \in SO(3)$, which is denoted as [17]

$$R_{ZXY}(\phi, \theta, \psi) = \begin{bmatrix} c_\psi c_\theta - s_\phi s_\psi s_\theta & -c_\phi s_\psi & c_\psi s_\theta + c_\theta s_\phi s_\psi \\ c_\theta s_\psi + c_\psi s_\phi s_\theta & c_\phi c_\psi & s_\psi s_\theta - c_\psi c_\theta s_\phi \\ -c_\phi s_\theta & s_\phi & c_\phi c_\theta \end{bmatrix} \tag{A-11}$$

The Z-X-Y Euler angles rotate $\{\mathcal{B}\}$, as can be seen in Figure A-1a. The first rotation by yaw angle ψ is around the z-axis of $\{\mathcal{I}\}$. Next is the rotation by roll angle ϕ, and the last rotation is by pitch angle θ.

The unit vector q from the QR to the load is represented in $\{\mathcal{B}\}$. Define ϕ_L as the rotation of the load around the z-axis, measured from $\vec{b}_1$, and θ_L is the angle between the cable and the z-axis of $\{\mathcal{B}\}$, see Figure A-1b. The Cartesian coordinates can be retrieved through

$$x_L = x_Q + qL \tag{A-12}$$

where

$$q = \begin{bmatrix} s_{\theta_L} c_{\phi_L} \\ s_{\theta_L} s_{\phi_L} \\ -c_{\theta_L} \end{bmatrix} \tag{A-13}$$

Differentiating Equation A-12 and A-13 gives

$$\begin{aligned} \ddot{x}_L &= \ddot{x}_Q + \ddot{q}L \\ \ddot{q} &= \begin{bmatrix} \ddot{\theta}_L c_{\theta_L} c_{\phi_L} - \ddot{\phi}_L s_{\theta_L} s_{\phi_L} - \dot{\phi}_L^2 s_{\theta_L} c_{\phi_L} - \dot{\theta}_L^2 s_{\theta_L} c_{\phi_L} - 2\dot{\theta}_L \dot{\phi}_L c_{\theta_L} s_{\phi_L} \\ \ddot{\theta}_L c_{\theta_L} s_{\phi_L} + \ddot{\phi}_L s_{\theta_L} c_{\phi_L} - \dot{\phi}_L^2 s_{\theta_L} s_{\phi_L} - \dot{\theta}_L^2 s_{\theta_L} s_{\phi_L} + 2\dot{\theta}_L \dot{\phi}_L c_{\theta_L} c_{\phi_L} \\ \ddot{\theta}_L s_{\theta_L} + \dot{\theta}_L^2 c_{\theta_L} \end{bmatrix} \end{aligned} \tag{A-14}$$

$$\begin{aligned} \ddot{x}_Q &= \frac{1}{m_Q}(f(c_\psi s_\theta + c_\theta s_\phi s_\psi) - T s_{\theta_L} c_{\psi_L}) \\ \ddot{y}_Q &= \frac{1}{m_Q}(f(s_\psi s_\theta - c_\psi c_\theta s_\phi) - T s_{\theta_L} s_{\psi_L}) \\ \ddot{z}_Q &= \frac{1}{m_Q}(f(c_\phi c_\theta) - T c_{\theta_L}) - g \end{aligned} \tag{A-15}$$

A-4 Figures

Figure A-2: Simulink Command Filter

A-5 MATLAB code

A-5-1 A MatlabListing

```
%
% Comment
%
n=10;
for i=1:n
    disp('Ok');
end
```

Bibliography

[1] R. P. K. Jain and T. Keviczky, "MSc Thesis: Transportation of Cable Suspended Load using Unmanned Aerial Vehicles: A Real-time Model Predictive Control approach," 2015.

[2] S. Sadr, S. Ali, A. Moosavian, and P. Zarafshan, "Dynamics Modeling and Control of a Quadrotor with Swing Load," *Journal of Robotics, Hindawi Publishing Corporation*, vol. 2014.

[3] T. Lee, M. Leok, and N. H. Mcclamroch, "Geometric Tracking Control of a Quadrotor UAV on SE(3)," *49th IEEE Conference on Decision and Control*, no. 3, pp. 5420–5425, 2010.

[4] F. Goodarzi, D. Lee, and T. Lee, "Geometric nonlinear PID control of a quadrotor UAV on SE (3)," *Control Conference (ECC), 2013 European*, pp. 3845–3850, 2013.

[5] K. Sreenath, N. Michael, and V. Kumar, "Trajectory generation and control of a quadrotor with a cable-suspended load - A differentially-flat hybrid system," in *Proceedings - IEEE International Conference on Robotics and Automation*, pp. 4888–4895, 2013.

[6] K. Sreenath, T. Lee, and V. Kumar, "Geometric control and differential flatness of a quadrotor UAV with a cable-suspended load," in *Proceedings of the IEEE Conference on Decision and Control*, pp. 2269–2274, 2013.

[7] S. Tang, "Aggressive Maneuvering of a Quadrotor with a Cable-Suspended Payload," tech. rep., University of Pennsylvania Philadelphia, Pennsylvania, 2014.

[8] N. Chaturvedi, "Rigid-Body Attitude Control," *IEEE Control Systems*, vol. 31, no. 3, pp. 30–51, 2011.

[9] R. M. Murray, Z. Li, and S. S. Sastry, *A Mathematical Introduction to Robotic Manipulation*, vol. 29. 1994.

[10] T. Lee, *Computational Geometric Mechanics and Control of Rigid Bodies*. PhD thesis, The University of Michigan, 2008.

[11] T. L. T. Lee, N. McClamroch, and M. Leok, "A lie group variational integrator for the attitude dynamics of a rigid body with applications to the 3D pendulum," *Proceedings of 2005 IEEE Conference on Control Applications, 2005. CCA 2005.*, pp. 962–967, 2005.

[12] T. Lee, M. Leok, and N. H. McClamroch, "Lagrangian mechanics and variational integrators on two-spheres," *International Journal for Numerical Methods in Engineering*, vol. 79, no. 9, pp. 1147–1174, 2009.

[13] T. Lee, M. Leok, and N. H. McClamroch, "Stable Manifolds of Saddle Points for Pendulum Dynamics on S^2 and SO(3)," p. 9, 2011.

[14] F. Bullo and A. D. Lewis, *Geometric control of mechanical systems: modeling, analysis, and design for simple mechanical control systems.* Springer, 2005.

[15] K. Sreenath, Taeyoung Lee, and V. Kumar, "Geometric control and differential flatness of a quadrotor UAV with a cable-suspended load," in *52nd IEEE Conference on Decision and Control*, pp. 2269–2274, IEEE, dec 2013.

[16] J. H. Gillula, H. Huang, M. P. Vitus, and C. J. Tomlin, "Design of guaranteed safe maneuvers using reachable sets: Autonomous quadrotor aerobatics in theory and practice," in *Proceedings - IEEE International Conference on Robotics and Automation*, pp. 1649–1654, 2010.

[17] R. Mahony, V. Kumar, and P. Corke, "Multirotor Aerial Vehicles: Modeling, Estimation, and Control of Quadrotor," *IEEE Robotics & Automation Magazine*, vol. 19, no. 3, pp. 20–32, 2012.

[18] J. A. Farrell, M. Polycarpou, M. Sharma, and W. Dong, "Command Filtered Backstepping," pp. 1923–1928, 2008.

[19] D. Mellinger and V. Kumar, "Minimum snap trajectory generation and control for quadrotors," in *Proceedings - IEEE International Conference on Robotics and Automation*, pp. 2520–2525, 2011.

[20] S. Tang and V. Kumar, "Mixed Integer Quadratic Program Trajectory Generation for a Quadrotor with a Cable-Suspended Payload," *IEEE International Conference on Robotics and Automation (ICRA)*, pp. 2216–2222, 2015.

Nomenclature

ϵ	Tuning parameter to enable rapid exponential convergence of e_R, e_Ω
$\lambda_M(\cdot)$	Maximum eigenvalue
ω_i	Angular speed of rotor i
$\{\mathbf{b}_1, \mathbf{b}_2, \mathbf{b}_3\}$	Unit vectors along the axes of $\{\mathcal{B}\}$
$\{\mathbf{c}_1, \mathbf{c}_2, \mathbf{c}_3\}$	Unit vectors along the axes of $\{\mathcal{C}\}$
$\{\mathbf{e}_1, \mathbf{e}_2, \mathbf{e}_3\}$	Unit vectors along the axes of $\{\mathcal{I}\}$
$\{\mathcal{B}\}$	Body Frame
$\{\mathcal{C}\}$	Intermediary Frame
$\{\mathcal{I}\}$	Inertial World Frame
b	Thrust factor
CM	Center of Mass
d	Drag factor
f	Total thrust. $f = \sum_{i=1}^{4} F_i$
F_i	Force generated by rotor i
g	Gravitation constant
L	Length of the cable
l	Distance from the rotor to the QR CoM
M	Total moment in $\{\mathcal{B}\}$. $M = \begin{bmatrix} M_\phi & M_\theta & M_\psi \end{bmatrix}^T$
M_i	Drag moment generated by each propellor

q	Unit vector from QR to Load
x_L	Position of the load
x_Q	Position of the of the QR CoM
x_{CM}	Position CM of QR-Load system

Acronyms

QR	Quadrotor
UAV	Unmanned Aerial Vehicle
CoM	Center of Mass
DOF	Degree of Freedom
PID	Proportional-Integral-Derivative (Controller)
MPC	Model Predictive Control
LQR	Linear Quadratic Regulator
QP	Quadratic Programming